The Astrophysical Journal, 834:20 (14pp), 2017 January 1 doi:10.3847/1538-4357/834/1/20

SPECTRAL ENERGY DISTRIBUTION MAPPING OF TWO ELLIPTICAL GALAXIES ON SUB-kpc SCALES

A. Amblard[1,2], P. Temi[1], M. Gaspari[3,5], and F. Brighenti[4]
[1] NASA Ames Research Center, Moffett Field, CA, USA
[2] BAER Institute, Sonoma, CA, USA
[3] Department of Astrophysical Sciences, Princeton University, Princeton, NJ 08544, USA
[4] Astronomy Department, University of Bologna, Via Ranzani 1, I-40127, Bologna, Italy
Received 2016 July 29; revised 2016 October 19; accepted 2016 October 28; published 2016 December 27

ABSTRACT

We use high-resolution *Herschel*-PACS data of two nearby elliptical galaxies, IC 1459 and NGC 2768, to characterize their dust and stellar content. IC 1459 and NGC 2768 have an unusually large amount of dust for elliptical galaxies ((1–3) $\times$ 10^5 $M_\odot$); this dust is also not distributed along the stellar content. Using data from *GALEX* (ultra-violet) to PACS (far-infrared, FIR), we analyze the spectral energy distribution (SED) of these galaxies with CIGALEMC as a function of the projected position, binning images in 7.″2 pixels. From this analysis, we derive maps of SED parameters, such as the metallicity, the stellar mass, the fraction of young stars, and the dust mass. The larger amount of dust in FIR maps seems related in our model to a larger fraction of young stars which can reach up to 4% in the dustier area. The young stellar population is fitted as a recent ($\sim$0.5 Gyr) short burst of star formation for both galaxies. The metallicities, which are fairly large at the center of both galaxies, decrease with the radial distance with a fairly steep gradient for elliptical galaxies.

Key words: galaxies: elliptical and lenticular, cD – galaxies: ISM – infrared: galaxies – infrared: ISM

1. INTRODUCTION

Early-type galaxies (ETGs) have long been thought to be depleted of any molecular or atomic gas and to produce a negligible amount of stars. However, recent advances in technology have allowed us to probe further the interstellar medium (ISM) of ETGs and to realize that a few ETGs harbor a substantial amount of gas (Wiklind & Henkel 1989; Lees et al. 1991; Wang et al. 1992; Wiklind et al. 1995; Young et al. 2011; Alatalo et al. 2013). ETGs generally have a complex multiphase ISM, which is a key component of the galactic ecosystem. Hot, warm, and cold gas detections have been reported by several authors (e.g., Caon et al. 2000; Mathews & Brighenti 2003; Ellis & O'Sullivan 2006; Sarzi et al. 2006, 2013; Mulchaey & Jeltema 2010; Davis et al. 2011; Serra et al. 2012). The cold ISM is often spatially extended, with irregular distribution and kinematics (Caon et al. 2000). Dust is also present in all the phases of the ISM (Temi et al. 2005, 2009; Smith et al. 2012), and the dust-to-gas ratio can be used to track down the origin of the cold gas. A multiphase ISM is expected to keep the galaxy "alive," allowing for (perhaps tiny) episodes of star formation (SF) and a sizable fraction of ETGs shows evidence of recent SF (Trager et al. 2000; Kaviraj et al. 2007). In some ETGs a fraction of cold gas is thought to have an external origin, as indicated by the misaligned kinematics of the cold gas (both ionized and neutral) with respect to the stars (e.g., Davis et al. 2011, and references therein). However, some ISM in the cold phase certainly comes from internal processes, such as stellar mass loss or hot gas cooling (Davis et al. 2011; David et al. 2014; Werner et al. 2014).

ETGs are viewed as the end step of galactic evolution; as such their proportion is increasing as the universe is aging and they contain important clues for how star formation evolved in galaxies. The proximity of some of these nearby objects is the perfect testing ground for theories, given the accessibility to high angular resolution and spectroscopy that some higher-redshift objects lack.

Numerical simulations show that ETGs can be produced from major mergers of late-type galaxies. During mergers, tidal interactions drive the gas into the center; this gas fuels a starburst and feeds the black hole (BH) growth. The gas consumption by the starburst and the BH feedback leave a merger remnant with a very low star formation rate (SFR) (Di Matteo et al. 2005; Springel et al. 2005a, 2005b; Hopkins et al. 2009). However, the merger rate needed to produce the correct amount of ETGs is larger than that estimated with the same simulations.

A first attempt to distinguish gas-rich and gas-poor ETGs split them in two separate groups, lenticular and ellipticals. Morphologically, lenticular galaxies still have a fairly large disk that does not present spiral arms, whereas elliptical galaxies are bulge-dominated. More recently, the ATLAS-3D survey has tried to separate more accurately two sub-class of ETGs, using the gas dynamics (Emsellem et al. 2011). They separate their ETGs sample into a slow-rotator category that roughly corresponds to giant ellipticals and a fast-rotator category that is composed mostly of lenticulars.

Lenticular galaxies seems to have a wider range of properties compared to ellipticals that resemble more the old definition of ETGs. However, even in ellipticals, large differences prevail. Recent observations of elliptical galaxies with *Spitzer* and *Herschel* (Temi et al. 2005, 2007a, 2007b, 2009; Smith et al. 2012; Agius et al. 2013; Mathews et al. 2013) have revealed that the far-infrared (FIR) luminosity $L_{\rm FIR}$ from these galaxies can vary by $\sim$100 among galaxies with similar optical luminosity. The 70 μm band luminosities (from Temi et al. 2007a, 2009), is a good example of such a huge scatter in the FIR luminosity of elliptical galaxies. Some of the high L_{70} galaxies are members of a small subset of ellipticals having radio detections of neutral and molecular gas. A few others may be S0 galaxies which, because of their rotationally supported disks, often contain large masses of cold gas and dust. Ellipticals containing large excess masses of dust and cold

[5] Einstein and Spitzer Fellow.

gas probably result from significant galaxy mergers in the past. However a fraction of elliptical galaxies appear to be completely *normal* but L_{70} in these galaxies still ranges over a factor of ∼30, far larger than can be explained by uncertainties in the estimate of the FIR spectral energy distribution (SED) due to local stellar mass loss. While a significant fraction of the cold gas mass in low- to intermediate-mass ETGs is thought to have an external, merger-related origin (e.g., Davis et al. 2011), in the most massive ETGs the cold gas phases are presumably generated internally (Davis et al. 2011; David et al. 2014; Werner et al. 2014). Mergers with gas- and dust-rich galaxies have often been suggested for the origin of dust in all elliptical galaxies (e.g., Forbes 1991). Although the merger explanation is almost certainly correct in some cases, mergers cannot explain most of the observed scatter in L_{70}. A crucial element in our understanding of the evolution of galaxies toward ETGs is the mutual role played by the major merging of galaxies and the secular star formation quenching. Neither of these scenarios yet accounts for all the observational evidence, and one could assume both contributing to some extent.

This paper concentrates on the study of two atypical elliptical galaxies, IC 1459 and NGC 2768, that contain a substantial amount of dust. Both galaxies have optical and near-IR (NIR) morphologies that resemble any large elliptical galaxies, and they both are fairly red. IC 1459 has a $B - V$ and $V - R$ color of 0.9 according to Forbes et al. (1995) and a $g - r$ color of 0.85 in the OmegaCAM survey; NGC 2768 has a $g - r$ color of 0.87 in the Sloan Digital Sky Survey (SDSS). However, a first hint of their peculiarity came from dust absorption images that showed unusual dust features (Malin 1985, pp. 27–32; Kim 1989; Forbes et al. 1995). Furthermore, observations of dust emission in the FIR revealed some larger than expected fluxes and unusual morphology (Temi et al. 2007a; Crocker et al. 2008).

In this paper, we utilize the recent data from the *Herschel* PACS photometer at 70 and 160 μm, which reached an unprecedented FIR high angular resolution of 6″ and 12″ respectively, to map the parameters from a stellar population synthesis (SPS) model with wide-band photometric observations from the UV to the FIR.

2. GALAXIES SAMPLED

2.1. IC 1459

IC 1459 is a massive elliptical galaxy E3 ($M_V = -21.19$, $D = 16.5\ h^{-1}$ Mpc) that belongs to a group of mostly spiral galaxies (group number 15 of Huchra & Geller 1982). It has a counter-rotating stellar core with a maximum rotation of about $170\ km\ s^{-1}$ at 2″ (0.15 kpc). The stellar mass of the counter-rotating core is about $10^{10}\ M_\odot$ (Franx & Illingworth 1988) and the outer region velocity goes up to $45\ km\ s^{-1}$ but in the opposite direction. Stellar shells at tens of kpc from the center and other peculiar isophotes were observed by Williams & Schwarzschild (1979), Malin (1985, pp. 27–32), Forbes et al. (1995), and quantified by Tal et al. (2009). This disturbed morphology has led to the hypothesis that IC 1459 accreted some external material in the past, probably from a merger (Cappellari et al. 2002).

IC 1459 hosts an active galactic nucleus (AGN) characterized by two strong symmetric radio jets (about 1 Jy at 1.4 GHz; Ekers et al. 1989; Slee et al. 1994; Tingay & Edwards 2015), whose activity may have been triggered by the same event that gave the galaxy its peculiar morphology and kinematics. IC 1459 has a strong low-ionization nuclear emission-line region (LINER) optical spectrum (Phillips et al. 1986). However *Chandra* observations of the supermassive black hole of IC 1459 show a weak X-ray source ($L_X = 8 \times 10^{40}\ erg\ s^{-1}$, 0.3–8 keV, Fabbiano et al. 2003) with a flux much lower than expected from a $2 \times 10^9\ M_\odot$ BH (10× lower than normal radio-loud galaxy, Cappellari et al. 2002). IC 1459 has also been found to be a gigahertz-peaked spectrum radio source (Tingay et al. 2003) with a peak frequency of 2.5 GHz and low power. Serra & Oosterloo (2010) found that IC 1459 has an SSP (single stellar population)-equivalent age of $3.5^{+1.7}_{-0.4}$ Gyr using spectral line data from Tal et al. (2009) and SSP models from Thomas et al. (2003). This age estimate is biased toward the age of the youngest population (Serra & Trager 2007) and is more an indication of the age of the young stars. Serra & Oosterloo (2010) gave a rough estimate of 0.5%–5% of the young stellar population (in mass) formed between 300 Myr and 1 Gyr ago. Prandoni et al. (2012) deduced a molecular gas mass of about $2.5 \times 10^7\ M_\odot$ using CO(2-1) observations taken with the Atacama Pathfinder Experiment telescope, while Serra & Oosterloo (2010) measured a H I mass of about $2.5 \times 10^8\ M_\odot$.

2.2. NGC 2768

NGC 2768 has been classified as an E6 galaxy in the third reference catalog of bright galaxies (RCC3, de Vaucouleurs et al. 1991), but Sandage & Bedke (1994) have reported the galaxy as an almost edge-on S0 galaxy in the Carnegie Atlas of Galaxies. The galaxy is part of the SAURON sample (Emsellem et al. 2007), where it is classified as a fast rotator with a single component in their stellar kinematic classification scheme.

NGC 2768 has a low-luminosity AGN with a LINER spectrum (Heckman 1980), a compact radio core (Nagar et al. 2005), and an X-ray source consistent with being a point source (Komossa et al. 1999); its X-ray luminosity is about $10^{40}\ erg\ s^{-1}$ (Boroson et al. 2011).

It is a fairly isolated galaxy (Wiklind et al. 1995) but has been associated with the Lyon Group of Galaxies (Garcia 1993). The effective radius of the galaxy is about 67″ (de Vaucouleurs et al. 1991), corresponding to 7.3 kpc at a distance of 22.4 Mpc (Tonry et al. 2001). Kim (1989) discovered a dust lane along the minor axis of NGC 2768, measured the rotation of the ionized gas around the major axis, and suggested an external origin of the gas in this galaxy. Crocker et al. (2008) traced the molecular gas of NGC 2768 with the CO(1-0) and (2-1) line emission, finding a molecular polar disc, coincidental with the dust absorption of Kim (1989). O'Sullivan et al. (2015) inferred a molecular gas mass of $2 \times 10^7\ M_\odot$ and Morganti et al. (2006) measured a H I mass of about $2 \times 10^8\ M_\odot$.

3. DATA

We base our work primarily on data obtained with the *Herschel Space Telescope* (Pilbratt et al. 2010) using the PACS instrument with the blue (70 μm) and red (160 μm) filters. In order to gather a larger amount of information in a self-consistent manner from the SED-fitting, we collect data from six additional instruments which span wavelengths from the UV to the FIR and have extensive sky coverage: *GALEX* for

the UV part, SDSS and OmegaCAM for the optical, Two Micron All Sky Survey (2MASS) and IRAC/MIPS-*Spitzer* for the NIR and mid-infrared (MIR).

3.1. UV Data

To cover the UV part of the spectrum we used *GALEX* GR6 data release.[6] *GALEX* surveys cover 25,000 deg^2 of the sky with a sensitivity down to $m_{AB} = 21$ for the All Sky Imaging Survey (AIS) and $m_{AB} = 25$ for the Deep Imaging Survey (DIS; Morrissey et al. 2007). *GALEX* is a NASA satellite, equipped with two microchannel plate detectors imaging in the near-UV (NUV) at 2271 Å and far-UV (FUV) at 1528 Å and a grism to disperse light for low-resolution spectroscopy. The source position accuracy is about 0.34 arcsec and the angular resolution of FUV and NUV is respectively 4.2 and 4.9 arcsec. We applied a galactic dust extinction correction, $A(\mathrm{FUV})/E(B-V) = 8.376$ $A(\mathrm{NUV})/E(B-V) = 8.741$, to the *GALEX* data, assuming Milky Way dust with $R_v = 3.1$ (Cardelli et al. 1989; Marino et al. 2011). UV emission is a good indicator of the dust content and SFR of galaxies when compared with optical data. NGC 2768 is a galaxy of the nearby galaxy survey that has a depth μ_{AB} of 28 mag/sq. arcsec; IC 1459 was observed by *GALEX* with the Guest Program Cycle 1 down to a similar depth. Both have been detected in the FUV and NUV.

3.2. Optical, NIR, and MIR Observations

The five SDSS bands cover the optical range of the SED and were observed on a large portion of the sky (14,555 deg^2). The SDSS data have an angular resolution of about 1.5 arcsec. We retrieved SDSS data through the Imaging Query Form interface.[7] N2768 has been observed in the five bands of the SDSS, *u*, *g*, *r*, *i* and *z* (respectively 0.335, 0.469, 0.616, 0.748, and 0.893 μm). Unfortunately, IC 1459 is too far south to have been observed by the SDSS; for this galaxy we used data from the OmegaCAM science archive.[8] This archive contains data obtained with the VLT Survey Telescope (VST) mostly from the VST ATLAS survey (Shanks et al. 2015). The VST ATLAS survey covers 4,500 deg^2 in the southern hemisphere at high galactic latitude with depth comparable to the SDSS and the same set of five filters. This archive contains images of IC 1459 in four filters *g*, *r*, *i* and *z*, with an angular resolution of about 0.8–1.0 arcsec. We applied a galactic dust extinction correction with the values provided on the NASA/IPAC Extragalactic Database (NED).[9] At NIR wavelength, we use the extended source catalog of the 2MASS data, which contains 1,647,599 sources. 2MASS resolution is about 2 arcsec and its source position accuracy is about 0.5 arcsec. The 10-σ limiting magnitude in the three filters *J*, *H*, K_s is about 14.7, 13.9, 13.1.[10] Both galaxies have counterparts in the three different filters, *J*, *H*, and K_s bands, at 1.24, 1.66, and 2.16 μm respectively.

The *Spitzer Space Telescope* provides data in the NIR with the IRAC camera with four channels imaging at 3.6, 4.5, 5.6, and 8 μm with about 2 arcsec angular resolution and in the MIR with the MIPS instrument observing at 24 μm (at longer wavelengths we used *Herschel* PACS) at an angular resolution of 6 arcsec (Rieke et al. 2004). We downloaded data for our galaxies from the NASA/IPAC Infrared Science Archive.[11]

3.3. FIR Observations

The launch of the *Herschel*[12] telescope allowed unprecedented precisions at FIR wavelength. We used public level2 data from the PACS instrument, downloaded from the *Herschel* Science Archive.[13] The PACS instrument observed at 70 and 160 μm (the 100 μm was not available for our sources) with an angular resolution of about 6 and 12 arcsec (Poglitsch et al. 2010). Level2 maps were combined into a single map for each object using a simple pixel co-addition technique. We subtracted from each image a background, estimated by taking a median at 3 arcmin around the source.

4. SED ANALYSIS

4.1. Data Pre-processing

In order to compare images taken by different instruments, each map was converted in units of Jy pixel^{-1} with a common angular resolution of 12″ and aligned so that they would cover the same area of the sky. The original angular resolution of each data set was taken as 4.″2 and 4.″9 for *GALEX*[14], 1.″4 for SDSS (median in *r*[15]), between 0.″8 and 1.″0 for OmegaCAM data (Shanks et al. 2015), about 2.″8 for 2MASS[16] 1.″66, 1.″72, 1.″88, 1.″98 for IRAC[17], 6″ for 24 μm MIPS[18], 5.″8 and 12.″0 for PACS (Poglitsch et al. 2010). For each wavelength, a convolution kernel was computed to bring the point-spread function to 12″ and each map was convolved using the appropriate kernel. To fit the SEDs of individual area, images were pixelated to 7.″2 to sample adequately the 12″ FWHM beam. Consequently neighbor pixels are slightly correlated.

4.2. SPS Model

To fit the SED of our galaxies, we use CIGALEMC[19] (Serra et al. 2011; Amblard et al. 2014) which is a modified version of the Code Investigating GALaxy Emission (CIGALE, Noll et al. 2009; Giovannoli et al. 2011). CIGALEMC uses a Markov Chain Monte Carlo sampling of the CIGALE parameters which allows one to increase the size of the parameter space covered and achieve a more efficient sampling of it. CIGALEMC uses the Maraston (2005) stellar population model and we use the Salpeter initial mass function (IMF) (Salpeter 1955).

The Salpeter IMF is in general a better match for massive ETGs as has been found previously (Grillo et al. 2009; Auger et al. 2010; Treu et al. 2010; Spiniello et al. 2011) using stellar dynamics and gravitational lensing. The Maraston (2005) stellar population model includes a realistic treatment of the

[6] http://galex.stsci.edu/GR6/
[7] http://skyserver.sdss3.org/dr9/en/tools/search/IQS.asp.
[8] http://osa.roe.ac.uk/
[9] http://ned.ipac.caltech.edu/
[10] http://www.ipac.caltech.edu/2mass/releases/allsky/doc/sec4_5.html
[11] http://sha.ipac.caltech.edu/applications/Spitzer/SHA
[12] *Herschel* is an ESA space observatory with science instruments provided by European-led Principal Investigator consortia and with important participation from NASA.
[13] http://herschel.esac.esa.int/Science_Archive.shtml
[14] http://www.galex.caltech.edu/researcher/techdoc-ch5.html
[15] http://www.sdss.org/dr3/
[16] http://www.sao.arizona.edu/FLWO/pairitel/seesum.html
[17] http://irsa.ipac.caltech.edu/data/SPITZER/docs/irac
[18] http://irsa.ipac.caltech.edu/data/SPITZER/docs/mips
[19] http://cigale.oamp.fr/

Table 1
Parameters Fitted by CIGALEMC to the Galaxy SEDs, with Priors Chosen

Parameters	Priors	Description
Z	$0.005 < Z < 0.07$	metallicity
t_{old}	$8.0 < t_{old} < 14$ Gyr	old star population age
τ_{old}	$0.5 < \tau_{old} < 3$ Gyr	old star population e-folding time
t_{young}	$0.1 < t_{young} < 4$ Gyr	age of the young stellar population
σ_{young}	$0.02 < \sigma_{young} < 1.5$ Gyr	time-spread of young stars
f_{young}	$0 < f_{young} < 1$	fraction of young stars
A_V	$0.01 < A_V < 5$ mag.	dust extinction in the V band
α	$0.2 < \alpha < 3.9$	slope of the dust mass over heating
f_{AGN}	$0 < f_{AGN} < 1$	AGN fraction of the dust luminosity
M_{gal}	$2 < M_{gal} < 11$	logarithm of the galaxy mass

thermally pulsating asymptotic giant branch (TP-AGB). The TP-AGB phase model is important for deriving an accurate stellar mass (Maraston et al. 2006; Ilbert et al. 2010). The metallicity Z is fitted with a uniform prior between 0.005 and 0.07; a previous attempt to fit our SEDs with a fixed solar metallicity did not return satisfactory fits.

When fitting the data, we assume an exponentially decreasing SFR for the old star population following Giovannoli et al. (2011). The age of the old stellar population is constrained between 8 and 14 Gyr and its e-folding time is constrained between 0.5 and 3 Gyr. The star formation history of the young stellar population is assumed to be Gaussian-shaped (Smith & Hayward 2015). The peak age is constrained to be between 0.1 and 4 Gyr and the width (σ) between 0.02 and 1.5 Gyr.

We use the Calzetti et al. (1994) and Calzetti (1997) attenuation to describe the dust absorption of starlight. We do not add any modification to the Calzetti curve, like a 2175 Å UV bump or a change of slope. The attenuation is modeled independently for the old and young stellar populations; the attenuation factor for the young population is A_V (V band attenuation) and there is a reduction factor f_V for the old stellar population ($A_V \times f_V$). For simplicity, here we assumed that both the old and young population have the same extinction, and fixed f_V to 1.

The IR emission from the dust is computed using Dale & Helou (2002) model, which is composed of 64 templates parameterized by a slope α. This slope represents the power-law slope of the dust mass over the heating intensity. Dale & Helou (2002) followed the Desert et al. (1990) approach by dividing their dust emission sources into large grains, small grains, and polycyclic aromatic hydrocarbons. They normalized these components using observations from IRAS, ISO, and SCUBA. In order to retrieve from α some commonly used quantities such as a dust temperature and a β index, we fit a relation between α, β, and T_d. This implies that our measurements of β and T_d are not fully independent, being linked by the Dale & Helou (2002) templates. CIGALEMC also includes a model for the AGN emission, using the AGN templates from Siebenmorgen et al. (2004b, 2004a) and a parameter for its amplitude f_{AGN}. The ten free parameters of the fit, Z, τ_{old}, t_{old}, σ_{young}, t_{young}, f_{young}, A_V, α, f_{AGN}, M_{gal}, are described in Table 1 along with their priors.

In the analysis of the SEDs, we use some derived parameters: SFR, M_* (the stellar mass) and M_d (dust mass); these are computed either from the fitted parameters and/or from the fitted SED. The SFR is computed from the contribution of the young and old stellar populations; however the young stellar population gives in general the dominant contribution. Therefore the SFR is mostly depending on the fitted parameters: the normalization M_{gal}, the fraction of young stars f_{young}, and the age of the young star population t_{young}. SFR increases with M_{gal} and f_{young}, and decreases slightly as young stellar population ages, i.e., as t_{young} gets larger. Apart from its M_{gal} dependency, the SFR is constrained by the UV, optical, and NIR part of the spectrum via the SPS of Maraston (2005).

M_* is calculated by integrating over the evolution track of the Maraston (2005) model, and depends primarily on the UV, optical, and NIR part of the spectrum, except for the overall normalization defined by M_{gal}. M_d is calculated from the dust parameter α, the dust absorption parameter A_V, and the mass of the galaxy M_{gal}.

4.3. NGC 2768 Analysis

At optical–NIR wavelengths the NGC 2768 morphology resembles an ellipsoid elongated in the R.A. direction, whereas in the MID to FIR the elongation migrates toward the decl. direction. The reported difference in the elongation direction is in agreement with observation of a polar (along the minor axis) ring/dust lane observed by Kim (1989) in $B - R$ color and by Crocker et al. (2008) in CO line emission. The CO lines show as well that this ring/disk is rotating (toward us in the south and away from us in the north). These results match the observation of the [O III] line from Sarzi et al. (2006) showing the same rotation of the ionized gas.

To understand the difference in gas and star content within NGC 2768, we split the galaxy into 144 areas, each covering 7.2×7.2 arcsec^2. In Figure 2, the grid of our 144 pixels is superimposed on a map of NGC 2768 from the 2MASS K-band and the PACS 160 μm band. The black numbers on the maps represent the pixel index, which increases from bottom to top and left to right (in the RADEC coordinate system, south to north then east to west).

Each pixel is then fitted with our SED model (Figure 4), and model parameters can be mapped throughout the galaxy. The constraints shown on each plot have been marginalized over the remaining set of parameters. Some parameters are poorly constrained, such as the age of the old stellar population and its e-folding time. Some others only have upper or lower limits such as the FIR luminosity fraction contributed by an AGN, or the duration of the recent starburst. Lastly, some parameters, like α and the age of the new stellar population, while well constrained, do not present a statistically significant variation across the map, and only their average value will be reported.

Figure 3 represents a set of constraints on a pixel of NGC 2768 (pixel #80, slightly above the central pixel, [x, y] coordinates [6, 8]) and shows the correlation between parameters. Overall most parameters are not very correlated. The strongest correlation is the anti-correlation between the fraction of young stars and the stellar mass. Another is the anti-correlation between the metallicity and the age of the young stellar population. These correlations widen our uncertainty on these parameters as constraints presented in this paper are marginalized over the value of all the other parameters.

The metallicity is one of the major constraints coming from our fluxes and models, in Figure 5 it is shown to decrease sharply with the radial distance from the center of the galaxy. The uncertainty in our metallicity measurements is from 0.003 to 0.005 (7%–16%). The shape of its distribution follows the

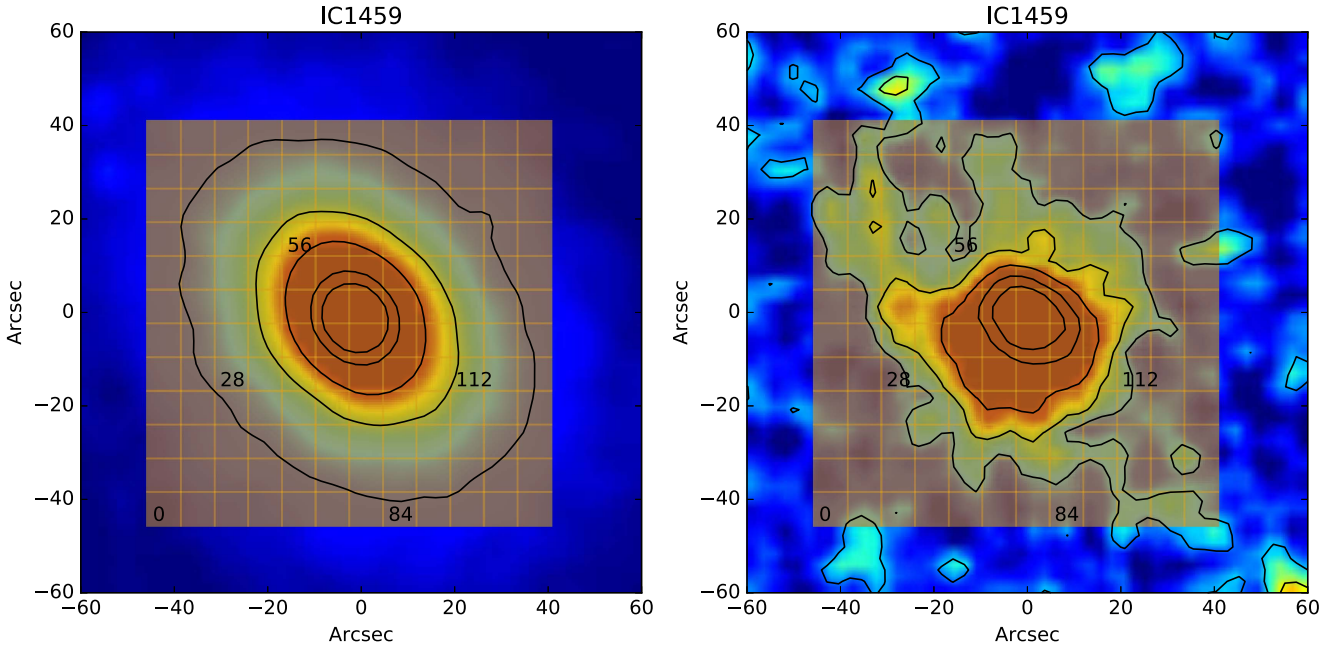

Figure 1. Left: 2MASS *K*-band image of IC 1459 with the grid of our 7.″2 pixels superimposed on top. Right: PACS 160 μm image of IC 1459 with the grid of our 7.″2 pixels superimposed on top. The black numbers in the grid represent the pixel index; it increases from bottom to top and left to right (in the RADEC coordinate system, the pixel index goes from south to north then east to west).

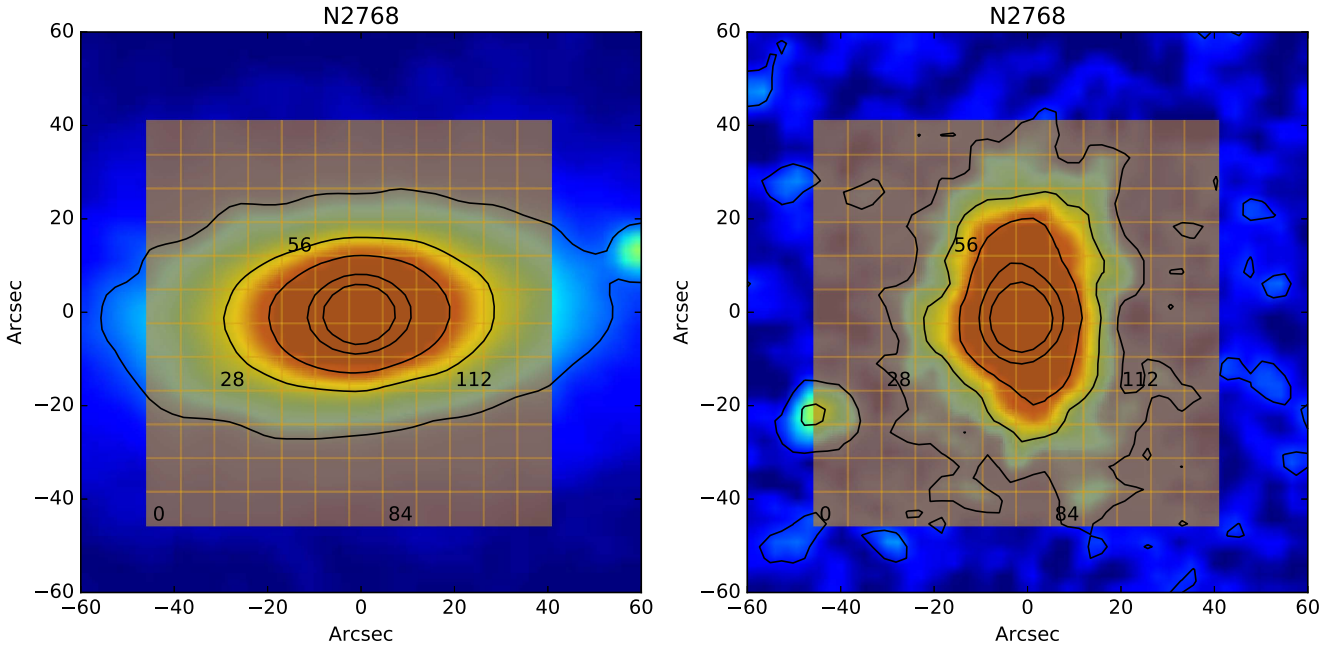

Figure 2. Left: 2MASS *K*-band image of NGC 2768 with the grid of our 7.″2 pixels superimposed on top. Right: PACS 160 μm image of NGC 2768 with the grid of our 7.″2 pixels superimposed on top. The black numbers in the grid represent the pixel index; it increases from bottom to top and left to right (in the RADEC coordinate system, the pixel index goes from south to north then east to west).

old stellar population, which is dominant in NGC 2768. The overall values of the metallicity, between 0.025 and 0.045, are in good agreement with measurements from Sil'chenko (2006), Howell (2005), and Denicoló et al. (2005), ranging from 0.02 to 0.048. Their measurements used Lick indices and SSP models from Thomas et al. (2003) to extract the age and metallicity of NGC 2768 within a radius of about 8″. Li et al. (2007) measured a metallicity of 0.031 ± 0.009 using $B-K$ and $B-V$ colors within the effective radius and Bruzual & Charlot (2003) SPS models with a Salpeter IMF. These results are also qualitatively in agreement with Foster et al. (2009), where the Ca triplet lines (between 8483 and 8677Å) were used to probe the metallicity from $r_e/8$ to $2r_e(r_e \simeq 64'')$ with the models of Vazdekis et al. (2003) using a Kroupa IMF. Foster et al. (2009) measured a lower metallicity, ranging from 0.002 to 0.02, but also found a decreasing metallicity with radius. Their slope in the first r_e is about −0.015 whereas ours is about −0.019 in Z (in $\delta\log(Z)/\delta\log(r/r_e)$ our slope is about −0.21, whereas theirs is about −0.6). Kuntschner et al. (2010), using Lick indexes and SSP models from Thomas et al. (2003), found a decreasing metallicity gradient going from 0.02 at $r_e/8$ to 0.013 at r_e, corresponding to a −0.007 gradient in *Z*.

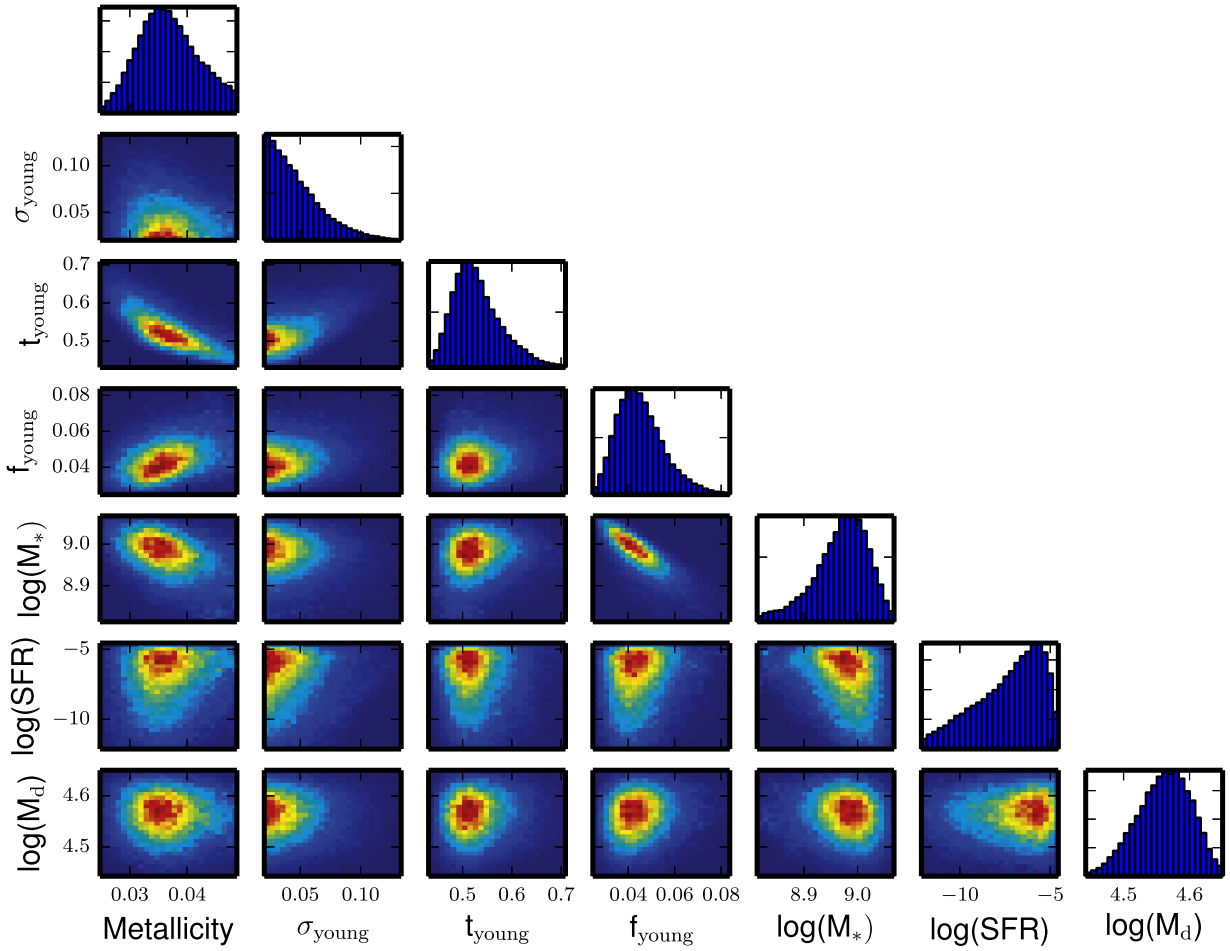

Figure 3. Constraints on the metallicity, $\sigma_{\rm young}$, $t_{\rm young}$, $f_{\rm young}$, log(M_*), log(SFR), and log(M_d) of the pixel 80 of NGC 2768. Most parameters plotted in this figure do not correlate strongly; the parameter pairs ($t_{\rm young}$, Metallicity) and ($f_{\rm young}$, log(M_*)) are slightly anti-correlated.

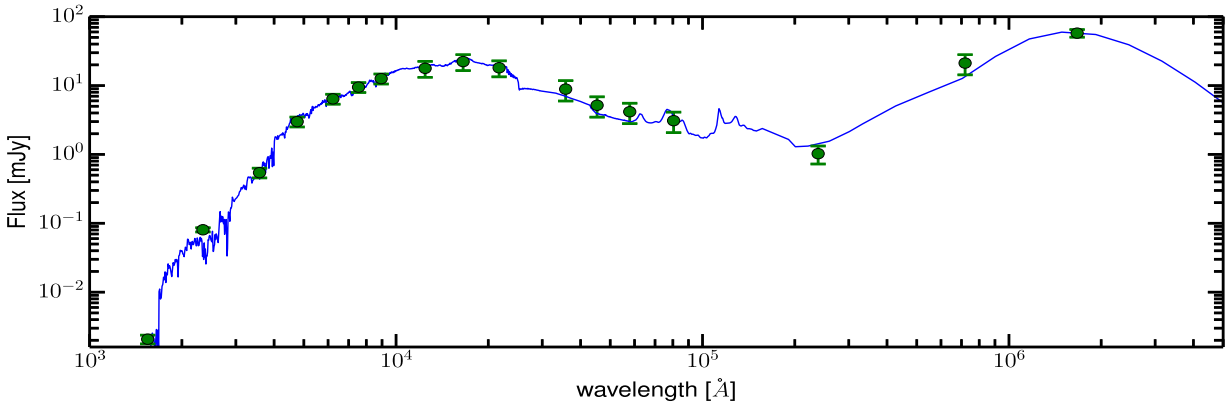

Figure 4. SED of the pixel 80 of NGC 2768; the blue solid line represents the best modeled SED; green dots represent data observed with *GALEX*, VST ATLAS, 2MASS, *Spitzer*, and *Herschel*.

The fraction of young stars fitted across NGC 2768 (Figure 6) is on average about 3.5% and peaks at about 5% in the polar regions where the dust ring is located. The central pixel of NGC 2768 has a young star fraction of about 2%. The average error on the determination of the young star fraction is fairly substantial at about 1%. The average age of the young stellar population is about 0.5 ± 0.05 Gyr; the duration (1σ of the Gaussian-shaped burst) of the recent burst of star formation is poorly constrained and only an average upper limit of about on 100 Myr (95% confidence level) is derived. Kuntschner et al. (2010) did not detect a younger stellar population using Hβ absorption, but the low sensitivity of Hβ absorption to a small fraction and recent star formation (RSF) (Crocker et al. 2008) could explain the difference with our results. The polar ring region shows a slightly larger age for the young stellar population (0.55 Gyr) but it is not significant given our uncertainties.

The age and duration of the old stellar population formation is unconstrained and marginalized over the prior range, from 8 to 14 Gyr for its age and 0.5–3 Gyr for its e-folding time. Other

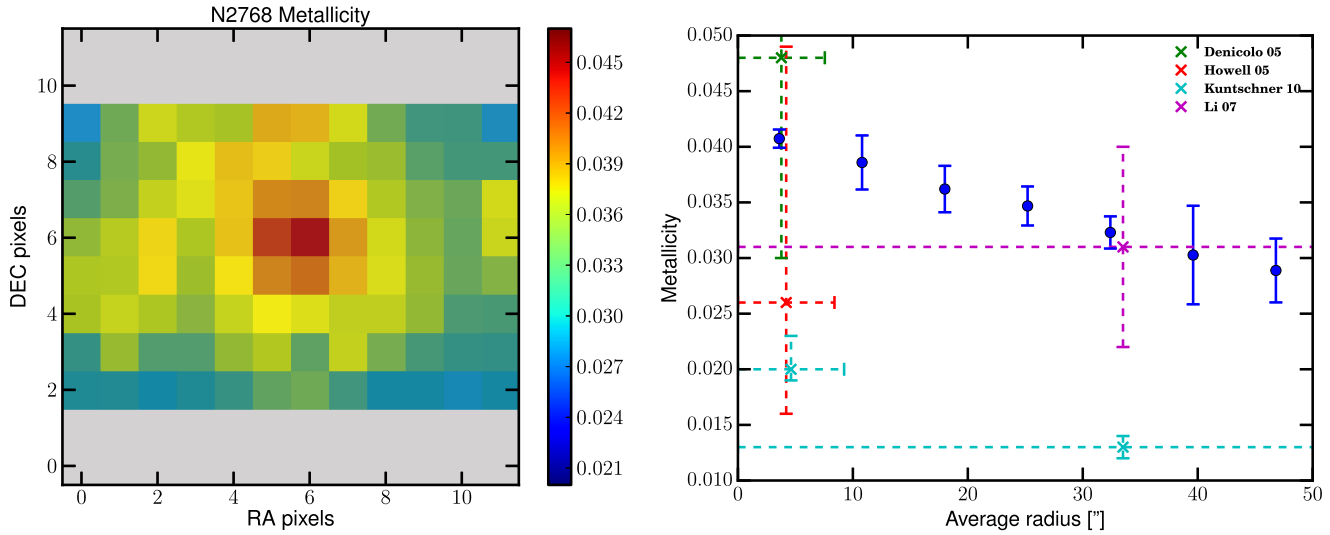

Figure 5. Left: metallicity of NGC 2768 within the 7.″2 pixel grid; unconstrained pixels are colored in gray, and the average error on the value of each pixel is about 0.004. Right: radial profile of the metallicity of NGC 2768 ($r_e = 64''$) with previous measurements from Denicoló et al. (2005), Howell (2005), Kuntschner et al. (2010), and Li et al. (2007). Error bars of our radial profile indicate the spread of the metallicity within the radial bin.

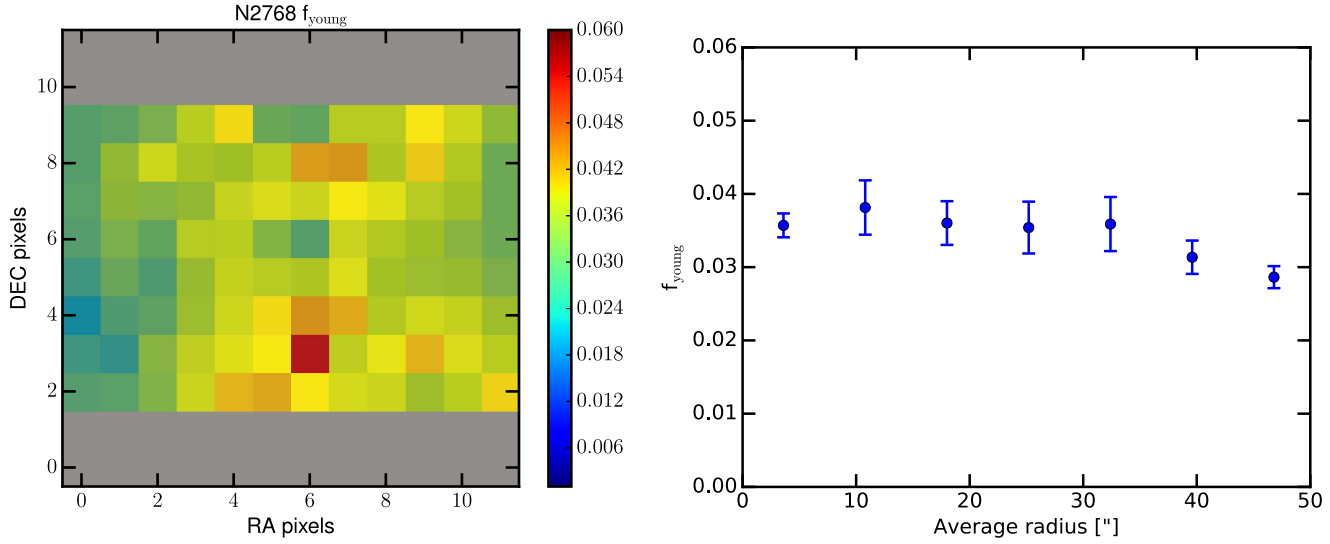

Figure 6. Left: young star fraction of NGC 2768 within the 7.″2 pixel grid; unconstrained pixels are colored in gray, and the average error on the value of each pixel is about 0.01. Right: radial profile of the young star fraction of NGC 2768 ($r_e = 64''$); error bars indicate the spread of the fraction within the radial bin.

studies have calculated an average age of the stellar population of NGC 2768; the results vary widely from 4 to 11 Gyr. Sil'chenko (2006) derived a luminosity-weighted mean age of 11 Gyr for the galaxy nucleus, Serra et al. (2008) found an age of 4 Gyr, and Zhang et al. (2008) estimated an age of about 6 Gyr. Howell (2005) derived an age of 10 Gyr with a large 7 Gyr uncertainty and Denicoló et al. (2005) calculated an age of 8.0 ± 3.5 Gyr, both within re/8.

$f_{\rm AGN}$, which represents the fractional contribution of a model of the AGN to the total FIR luminosity, is constrained to be lower than 2% across the entire galaxy at a 95% confidence level. The Dale & Helou (2002) model parameter α can only be given a lower limit of about 2.7 across the galaxy at a 95% confidence level. The recent SFR is not very well constrained because the dominant term in the SF history model is the old stellar population term whose parameters are not well constrained. Given the amplitude of the uncertainties, the residual SFR is the same across the galaxies at a rate of $10^{-7.5\pm2.0}\ M_\odot\ {\rm yr}^{-1}\ {\rm pixel}^{-1}$.

Figure 7 shows the reconstructed star formation history at the location of pixel # 80 in our parameter maps; the blue and red contours indicate respectively the 68% and 95% confidence levels. The $t = 0$ SFR is not well constrained and is dominated by the residual star formation from the exponential decrease. This SFR component is not well correlated with the dust distribution, which follows the SFR of the burst of young stars. The burst of young stars at about 0.5 Gyr is detected at a significant level above the expected old stellar population SFR. The amplitude of this burst is better constrained than the present-day SFR.

The dust absorption $A_{\rm V}$ is constrained at the center of the galaxy along the polar ring as seen in Figure 8. $A_{\rm V}$ peaks at about 0.07 mag in the galaxy center and decreases rapidly away from the polar ring. Further away the 95% confidence level upper limit is about 0.013. The dust absorption in V band is well correlated with the PACS 160 μm image, indicating a good consistency between the dust absorption near optical wavelengths and emission in the FIR.

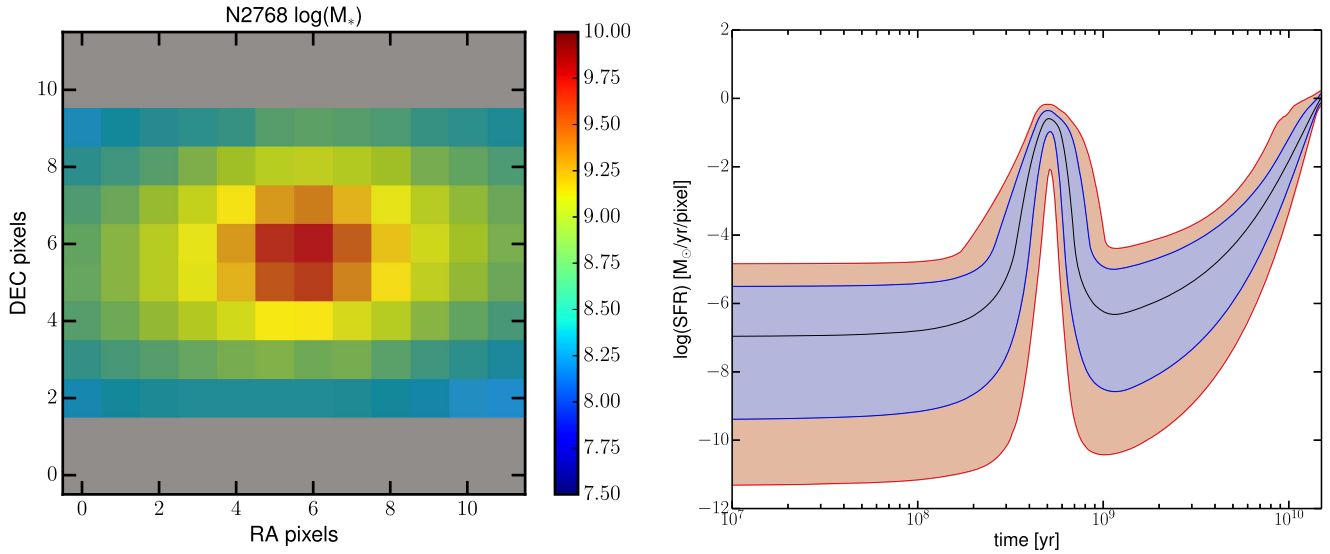

Figure 7. Left: logarithm of the stellar mass of NGC 2768 within the 7.″2 pixel grid; unconstrained pixels are colored in gray, and the average error on the value of each pixel is about 0.04. Right: star formation history of pixel #80 as modeled with a Gaussian-shaped burst and an exponential decrease; the blue contour represents the 68% confidence interval and the red contour represents the 95% confidence interval. The star formation rate is best constrained around the peak of the burst.

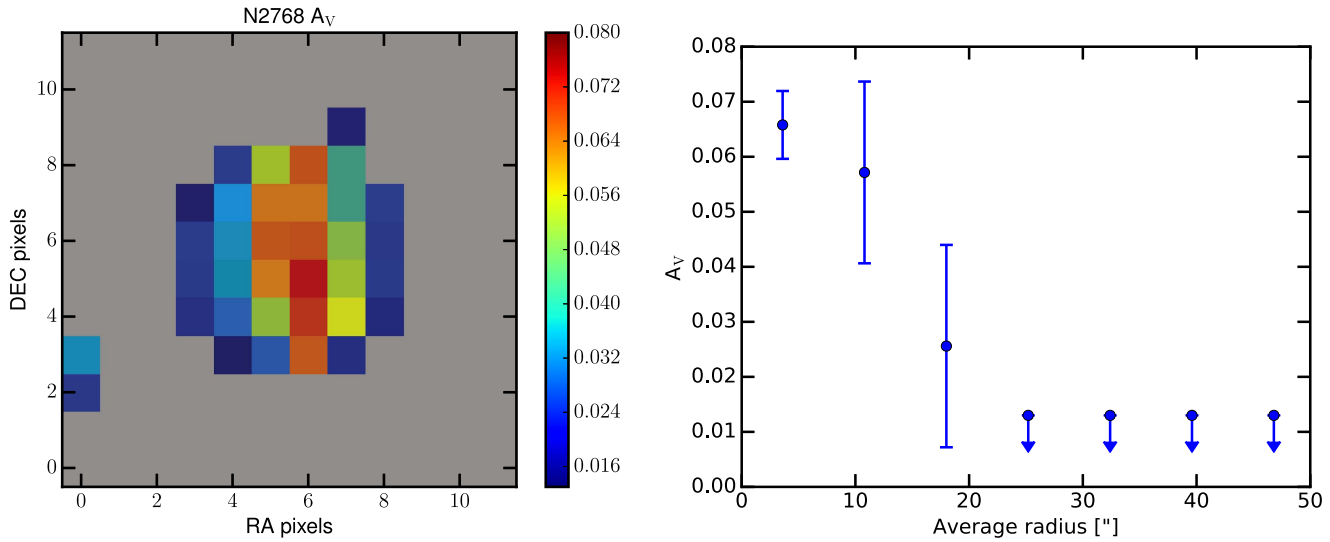

Figure 8. Left: dust absorption in the *V* band of NGC 2768 within the 7.″2 pixel grid; unconstrained pixels are colored in gray, and the average error on the value of each pixel is about 0.005. Right: radial profile of dust absorption of NGC 2768 ($r_e = 64''$); arrows indicate upper limits and error bars indicate the spread of the dust absorption within each radial bin.

Figure 9 reveals a dust mass distribution that is, as expected, also correlated with the PACS 160 μm image. The dust mass radial profile slope is about -0.09 dex arcsec^{-1}.

4.4. IC 1459 Analysis

IC 1459 has a very regular ellipsoidal morphology elongated along the north-west direction in the *K* band (Figure 1), but its PACS 160 μm image shows that the gas does not follow the stellar content and has a much more disturbed morphology. In addition to the dust located at its center, IC 1459 has large strip of dust lining from the south-east to the north-west on its west side. Goudfrooij et al. (1990) identified some potential spiral arms in Hα maps of IC 1459 that extend about 40″ away from its center. The location of the two largest Hα arms seems to coincide with the location of the structures present north of the galaxy center in the 160 μm map, although the FIR structures do not resemble closely the shape of spiral arms.

To differentiate the evolution and content of different regions of IC 1459, we split the galaxy into 144 areas, each covering 7.2 arcsec^2 in the same fashion as for NGC 2768. In Figure 1, the grid of our 144 pixels is superimposed on a map of IC 1459 from the 2MASS *K*-band and the PACS 160 μm band. The black numbers on the maps represent the pixel index, which increases from bottom to top and left to right (in the RADEC coordinate system, from south to north then east to west). Each pixel is then fitted with our SED model, as for NGC 2768, and constraints shown on each plot have been marginalized over the remaining set of parameters.

The fitted metallicity map (Figure 10) reveals high metallicity values roughly along the direction of the major axis of IC 1459, where metallicity is on average 0.044 compared to a metallicity of about 0.042 for neighboring pixels. On the other hand, the south-west side of this strip has a lower metallicity than its opposite side (0.037 versus 0.042).

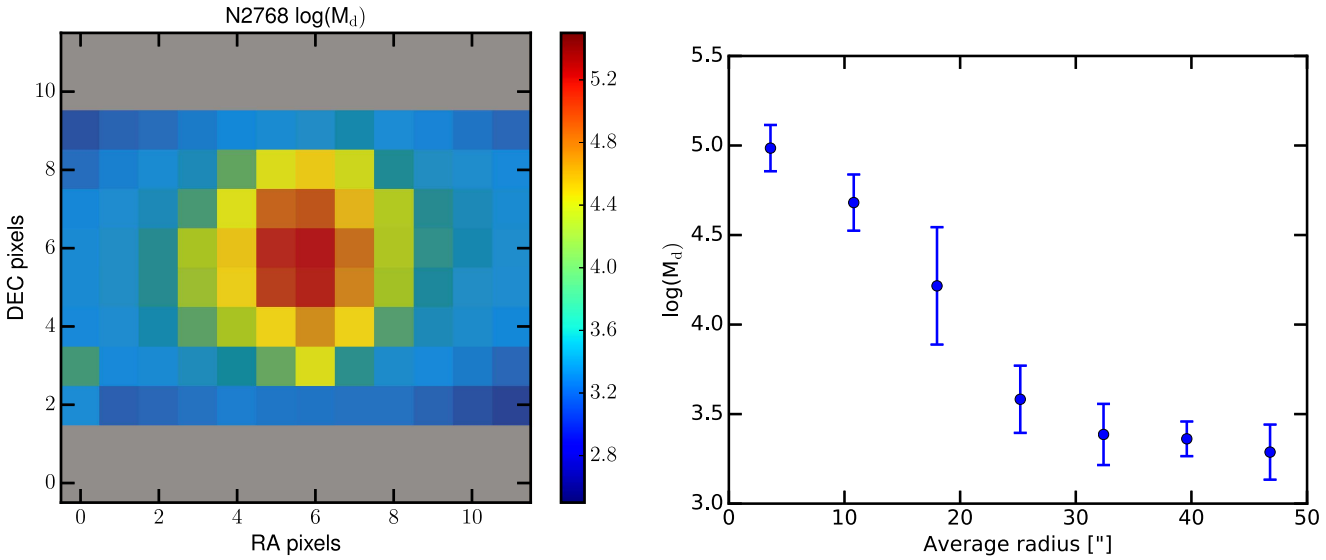

Figure 9. Left: dust mass of NGC 2768 within the 7.″2 pixel grid; unconstrained pixels are colored in gray, and the average error on the value of each pixel is about 0.06. Right: dust mass of NGC 2768 ($r_e = 64''$); error bars indicate the spread of the dust mass within each radial bin.

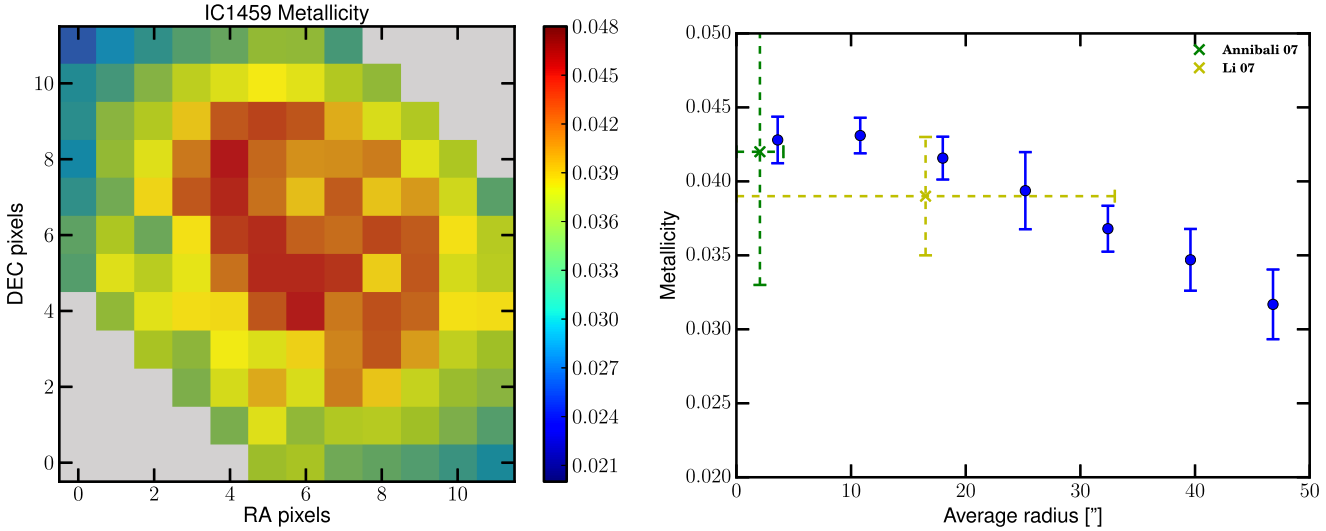

Figure 10. Left: metallicity of IC 1459 within the 7.″2 pixel grid; unconstrained pixels are colored in gray, and the average error on the value of each pixel is about 0.003. Right: radial profile of the metallicity of IC 1459 ($r_e = 33''$); error bars indicate the spread of the metallicity within each radial bin (error on each measurements is about 0.003). Previous measurements from Annibali et al. (2007), and Li et al. (2007) are shown with different colors.

This south-west side corresponds to the location of the extended structure in PACS 160 μm map. Overall IC 1459's metallicity is decreasing with the radial distance from its center beyond 15″ at a rate of −0.012 per effective radius in Z (about −0.36 in [Z/H] and about −0.39 in the $\delta\log(Z)/\delta\log(r/r_e)$). Annibali et al. (2007), using Lick indices and a SSP model, found a metallicity of 0.042 ± 0.009 at the center of IC 1459 ($r < r_e/8$). Cappellari et al. (2002) found a color gradient that could be explained by a metallicity gradient. Li et al. (2007) measured a metallicity of 0.039 ± 0.004 using $B-K$ and $B-V$ colors within the effective radius and Bruzual & Charlot (2003) SPS models with a Salpeter IMF. Our measured metallicity profile is shown in Figure 10 to be in good agreement with these previous measurements.

In Figure 11, the fraction of young stars fitted across IC 1459 is on average about 3% and peaks at about 4% in the south-west strip corresponding to the lower metallicity and the PACS 160 μm map arm. The central pixel of IC 1459 has a young star fraction of about 2.5%. The average error on the determination of the young star fraction is fairly substantial at about 0.5%. The age and duration of the old stellar population formation is unconstrained and marginalized over the prior range, from 8 to 14 Gyr for its age and 0.5–3 Gyr for its e-folding time.

The average age of the young stellar population is about 0.4 Gyr (Figure 12) with a typical error of 30 Myr; the duration (1σ of the Gaussian-shaped burst) of the recent burst of star formation is poorly constrained and only upper limits of about 80 Myr on average (95% confidence level) are derived.

Raimann et al. (2001) modeled the age and metallicity of stars in IC 1459 and found that 70% of the stars on the outskirts ($r > 20''$) and 90% of the stars in the center ($r < 4''$) have an age of 10 Gyr with a solar metallicity. These results hint at a younger population on the outskirts and a larger metallicity at the center, similarly to our results. Li et al. (2007) found an average age of 4.9 ± 1.2 Gyr, that is hard to compare to our model. Serra & Oosterloo (2010) found that IC 1459 has a

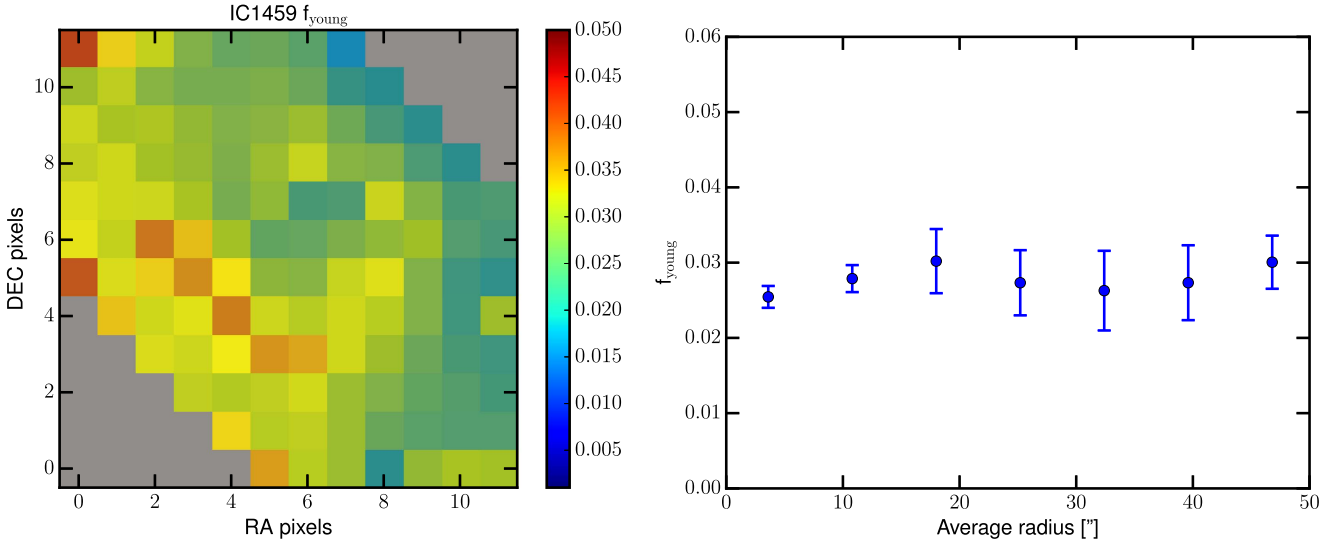

Figure 11. Left: fraction of young stars in IC 1459 within our grid of 7.″2 pixels; the average error on the derived values is about 0.005 (about 18%). Right: radial profile of the young stellar population fraction in IC 1459; error bars indicate the spread of the young stellar population fraction within each radial bin (error on each measurements is about 0.005).

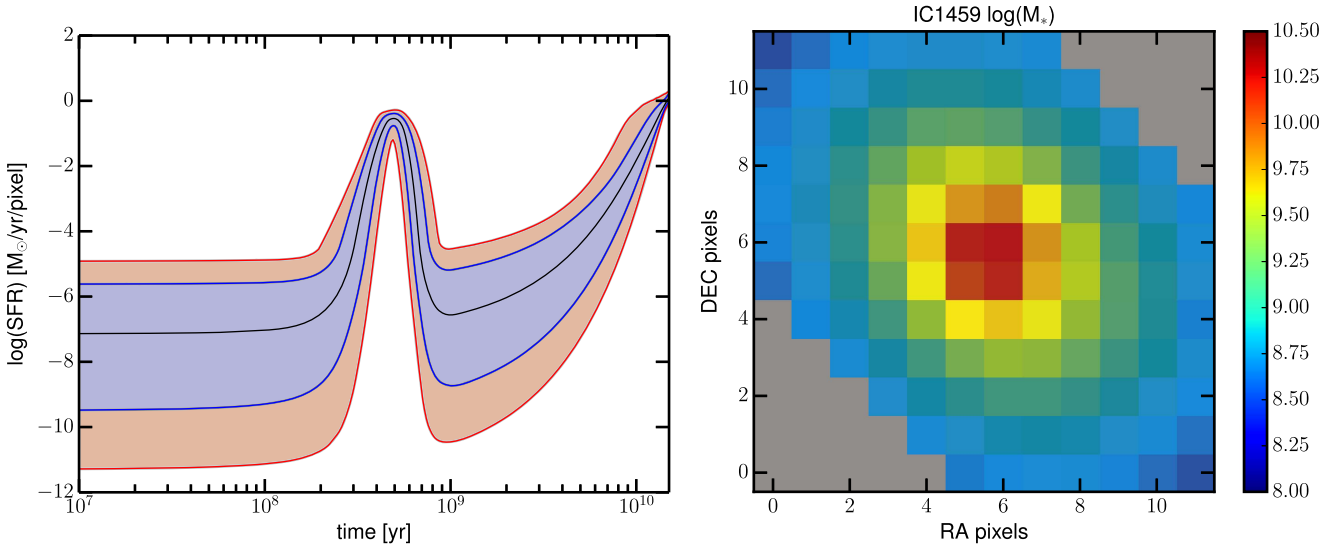

Figure 12. Left: SFR history of the pixel #30 of IC 1459; the blue contour represent the 68% confidence level interval and the red contour represents the 95% confidence level interval. Right: stellar mass in IC 1459 within our grid of 7.″2 pixels; the average error on the derived values is about 0.04 dex.

SSP-equivalent age of $3.5^{+1.7}_{-0.4}$ Gyr using spectral line data from Tal et al. (2009) and SSP models from Thomas et al. (2003). This age estimate is biased toward the age of the youngest population (Serra & Trager 2007) and is more an indication of the age of the young stars. Serra & Oosterloo (2010) gave a rough estimate of 0.5%–5% of the young stellar population (in mass) formed between 300 Myr and 1 Gyr ago, which is in good agreement with our own.

$f_{\rm AGN}$, which represents the fractional contribution of a model of the AGN to the total FIR luminosity, is constrained to be lower than 10% at a 95% confidence level where the FIR fluxes are quite large (i.e., PACS 160 μm map in Figure 1). Elsewhere the constraints on $f_{\rm AGN}$ are poorer and only a 20%–25% upper limit can be calculated.

The Dale & Helou (2002) model parameter α is measured to be 2.0 ± 0.1 in the central part of the galaxy (within a 15″ radius) and only constrained to be higher than 2.8 (95% confidence level) elsewhere. The measured α translates into a measured dust temperature at the center of the galaxy (15″ radius) of 21.5 ± 0.9 K and an emissivity index of 2.2 ± 0.1.

The dust absorption in the V band shown in Figure 13 is constrained to be around 0.04 mag where PACS 160 μm is the largest, reaching about 0.06 at the center of the galaxy. This correlation shows the consistency between the dust absorption near optical wavelengths and emission in the FIR. Figure 14 shows a dust mass distribution that is, as expected, also correlated with the PACS 160 μm image. The dust mass radial profile slope is about -0.04 dex arcsec^{-1}.

5. DISCUSSION

NGC 2768 and IC 1459 are elliptical galaxies with unusually large dust content as probed by dust absorption and emission. The model of SPS, which we used in this work, interprets this additional dust as due to a recent short burst of star formation that leads to an additional 3%–4% stellar mass. The timescale of our bursts is short, less than about 100 Myr (1 $\sigma_{\rm young}$ at 95%

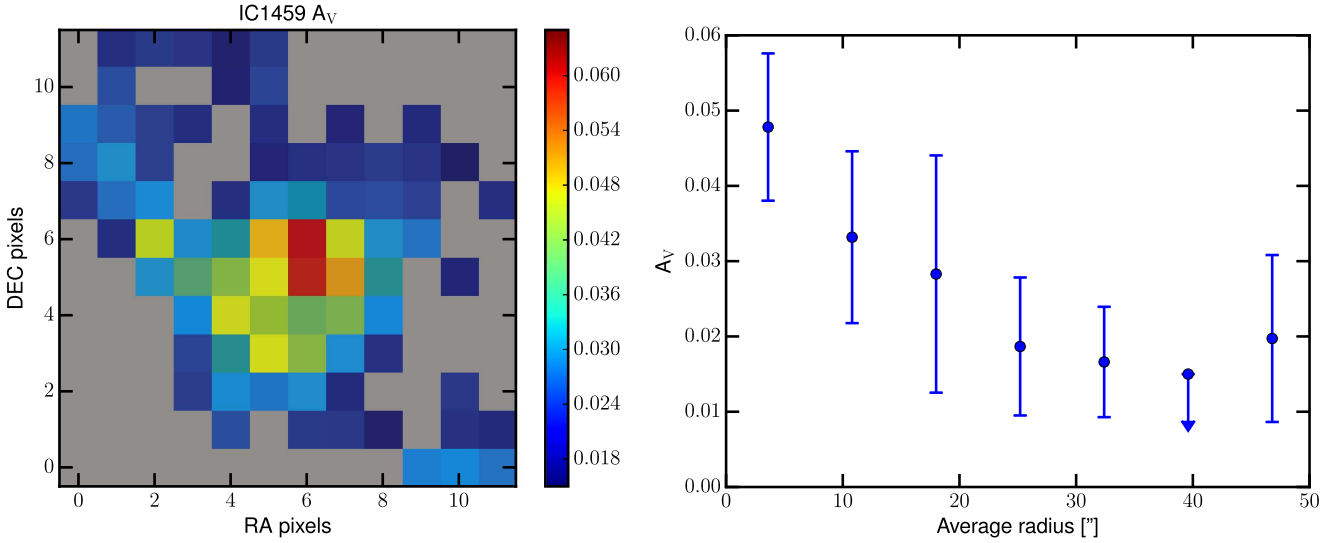

Figure 13. Left: dust absorption in the V band of IC 1459 within the $7\farcs2$ pixel grid; unconstrained pixels are colored in gray, and the average error on the value of each pixel is about 0.004. Right: radial profile of the dust absorption of IC 1459 ($r_e = 64''$); error bars indicate the spread of the dust absorption within each radial bin.

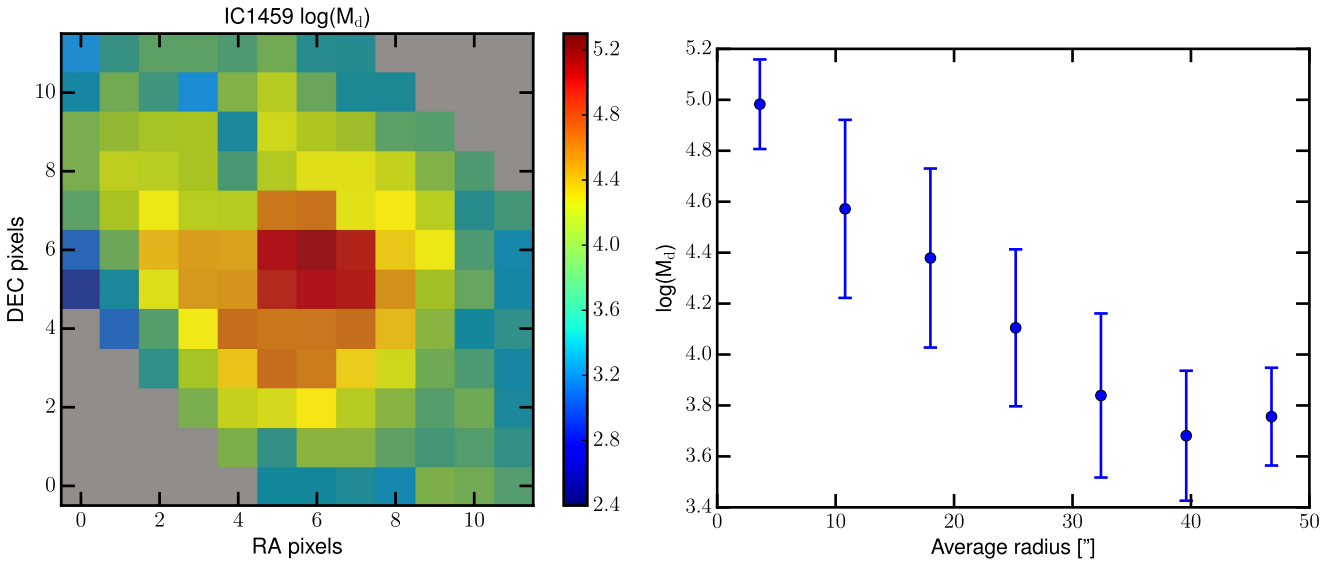

Figure 14. Left: dust mass of IC 1459 within the $7\farcs2$ pixel grid; unconstrained pixels are colored in gray, and the average error on the value of each pixel is about 0.1. Right: radial profile of the dust mass of IC 1459 ($r_e = 64''$); error bars indicate the spread of the dust mass within the radial bin.

c.l., FWHM would be about 250 Myr). Di Matteo et al. (2007, 2008) calculated from numerical simulation of galaxy collisions, that most mergers produce a star formation burst of less than 500 Myr (the duration is calculated during a period where the burst at least doubles the "normal" SFR). Di Matteo et al. (2007, 2008) also computed that most galaxy mergers produce a maximum rate of about 25 $M_\odot\,\mathrm{yr}^{-1}$ with a median of 10 $M_\odot\,\mathrm{yr}^{-1}$, the maximum SFR surface density being modeled at 10^2 to $10^3\,M_\odot\,\mathrm{yr}^{-1}\,\mathrm{kpc}^{-2}$. Our fit on the IC 1459 SED returns a value of about 30 $M_\odot\,\mathrm{yr}^{-1}$ for the total maximum SFR, which is a little high compared to Di Matteo et al.'s (2007) simulations. The highest SFR surface density for IC 1459 is 6 $M_\odot\,\mathrm{yr}^{-1}\,\mathrm{kpc}^{-2}$ and is more in line with these simulations. NGC 2768's total maximum SFR for the young star burst is about 10 $M_\odot\,\mathrm{yr}^{-1}$ and the maximum SFR surface density is 1 $M_\odot\,\mathrm{yr}^{-1}\,\mathrm{kpc}^{-2}$. Both estimates of the maximum SFR and SFR density are assuming the 95% confidence level upper limit on the duration of the recent SF burst, and therefore they constitute lower limits. The IC 1459 SF burst is a little large compared to most mergers simulated in Di Matteo et al. (2007), except for a retrograde merger between giant ellipticals.

Another possibility would be that the gas producing the recent burst of star formation has an internal origin, contrary to the external source of the merger hypothesis. Gaspari et al. (2015) explored how the AGN interactions with the hot and cold gas could produce "in-situ condensation of the hot gas via radiative cooling and nonlinear thermal instability." The condensation of the hot gas could produce an episode of SF and the AGN feedback would disturb the gas morphology, producing filamentary gas structures misaligned with the stellar distribution (Gaspari et al. 2012). Our SF history model is not a good representation of this model, but it tells us that the most recent significant burst of SF is about 0.5 Gyr and lasted less than 100 Myr. In the chaotic cold accretion of Gaspari et al. (2012), the gas cooling duration appears to be short ($\tilde{1}$00 Myr) and seems compatible with the short burst of SF measured.

Kaviraj et al. (2007) explored the UV color of a large catalog of elliptical galaxies, and found that most ellipticals with blue UV

color (NUV-r < 5.5) had an episode of RSF mostly within the last Gyr which led to about an additional 1% of young stars in mass. They also ran some merger models that can reproduce the NUV-r color distribution and give an average fraction of young star of about 1.4% and an average age of 0.6 Gyr. They also attempted to reproduce their data with a monolithic evolution model (Ferreras & Silk 2000), where the gas producing the RSF episode is coming from the mass loss of the old stellar population, but the RSF can only produce 0.5% of young stars and does not reproduce the NUV-r color distribution. NGC 2768 and IC 1459 have a blue NUV-r color (5.3 and 4.5 respectively) and our results match quantitatively the results of Kaviraj et al. (2007) with a fraction of young stellar mass on the higher range.

With values between 0.025 and 0.05, the metallicities of our galaxies are consistent with most previous measurements for these galaxies and with the average metallicity of nearby elliptical galaxies (Denicoló et al. 2005; Howell 2005; Sil'chenko 2006; Annibali et al. 2007; Li et al. 2007). The metallicity gradients are also consistent with previous measurements for NGC 2768 and IC 1459 and with measurements of other ETGs (Sánchez-Blázquez et al. 2007; Spolaor et al. 2009, 2010; Kuntschner et al. 2010; Rawle et al. 2010; Tortora et al. 2010; Koleva et al. 2011; La Barbera et al. 2011), with a medium to high negative gradient of -0.21 and -0.39 for NGC 2768 and IC 1459 respectively.

For instance, Koleva et al. (2011) found an average gradient for elliptical galaxies between 1 and 3 r_e of -0.26 ± 0.08 using optical spectra and SSP models generated by Pegase.HR (Le Borgne et al. 2004).

The metallicity gradients obtained for our two galaxies may be considered small for a quiescent evolution (Larson 1976; White 1980; Carlberg 1984; Kawata 2001; Kobayashi 2004) where calculated gradients range between -0.5 to -1 for massive elliptical galaxies, the idea being that in the monolithic collapse, the outer part of the galaxy cannot withhold the gas as long as the central part of the galaxy. The central part is therefore fueled by more metal-rich gas able to create stars of higher metallicity in the later stages of the SF history. Recently however, some other studies (Pipino et al. 2008, 2010; Tortora et al. 2013) have found that the lower range of metallicity is compatible with quiescent evolution of elliptical galaxies. Tortora et al. (2013) explained the discrepancy by a high [α/Fe] in the core of galaxies that shortens the SF and decreases the age gradients. In Pipino et al. (2010), the average metallicity gradient is also quite large at -0.3 with a spread growing with the galaxy mass, while the SF efficiency seems to influence the gradient value for larger galaxies (larger efficiency returning more negative gradient). On the other hand, metallicity gradients in post wet-merger galaxies are expected to be smaller at about a value of -0.2 to -0.3 (Kobayashi 2004; Hopkins et al. 2009).

Tortora et al. (2010), using a large sample of ETGs, found that galaxies with the oldest stellar populations have the largest metallicity gradient. The relation has a large dispersion but it would indicate that IC 1459 with a gradient of -0.39 has a stellar population age greater than 8 Gyr.

Tortora et al. (2010) found that color gradient in massive early-type galaxies ($M^* > 10^{11} M_\odot$) are quite shallow compared to the gradient in late-type galaxies or less massive early types. They found that these color gradients are mostly due to the metallicity gradient (age gradient being the second factor). Their minimum metallicity gradient reached -0.5 for these massive ETGs.

6. CONCLUSIONS

NGC 2768 and IC 1459 are elliptical galaxies with an unusually large amount of dust, seen in absorption and emission. In both cases, the dust spatial distribution does not follow the stellar mass distribution. NGC 2768 dust is distributed along the minor axis in what is possibly a ring, IC 1459 dust is distributed in some arms elongated from the center of the galaxy, either along the major axis or at a roughly 30 degree angle from the major axis.

Using multi-wavelength coverage on NGC 2768 and IC 1459 from UV to FIR, we modeled the SED using the Maraston SPS and SF history consisting of an exponentially decreasing old stellar population and a Gaussian-shaped young stellar formation burst. From the parameters of our model, we derived that the dust distribution is associated with a larger fraction of young stars ($\sim$3%), that were produced in a short burst ($<$100 Myr) about 0.5 Gyr ago. The dust mass distributions follow the FIR maps for both galaxies, and are therefore correlated with the fraction of young stars. For both galaxies, the dust absorption location in the V band is in good agreement with the dust emission. The age and duration of the older stellar population are not well constrained. These results are compatible with a recent merger but do not rule out an internal source for this recent burst of SF.

The metallicity of both galaxies is well constrained within a 50″ radius around the center and the gradients are found to be -0.21 and -0.39 respectively for NGC 2768 and IC 1459. These gradients and metallicities are consistent with previous measurements and typical values for elliptical galaxies.

This publication makes use of data products from the Two Micron All Sky Survey, which is a joint project of the University of Massachusetts and the Infrared Processing and Analysis Center/California Institute of Technology, funded by the National Aeronautics and Space Administration and the National Science Foundation. This publication makes use of data from SDSS-III. Funding for SDSS- III has been provided by the Alfred P. Sloan Foundation, the Participating Institutions, the National Science Foundation, and the U.S. Department of Energy Office of Science. The SDSS-III web site is http://www.sdss3.org/. SDSS-III is managed by the Astrophysical Research Consortium for the Participating Institutions of the SDSS-III Collaboration including the University of Arizona, the Brazilian Participation Group, Brookhaven National Laboratory, University of Cambridge, Carnegie Mellon University, University of Florida, the French Participation Group, the German Participation Group, Harvard University, the Instituto de Astrofisica de Canarias, the Michigan State/Notre Dame/JINA Participation Group, Johns Hopkins University, Lawrence Berkeley National Laboratory, Max Planck Institute for Astrophysics, Max Planck Institute for Extraterrestrial Physics, New Mexico State University, New York University, Ohio State University, Pennsylvania State University, University of Portsmouth, Princeton University, the Spanish Participation Group, University of Tokyo, University of Utah, Vanderbilt University, University of Virginia, University of Washington, and Yale University. This work is based in part on observations made with the *Spitzer Space Telescope*, which is operated by the Jet Propulsion Laboratory, California Institute of Technology under a contract with NASA. This work is based in part on observations made with the NASA *Galaxy Evolution Explorer*. *GALEX* is operated for

NASA by the California Institute of Technology under NASA contract. This research has made use of the NASA/IPAC Extragalactic Database (NED) which is operated by the Jet Propulsion Laboratory, California Institute of Technology, under contract with the National Aeronautics and Space Administration. MG is supported by NASA through Einstein Postdoctoral Fellowship Award Number PF-160137 issued by the *Chandra X-ray Observatory* Center, which is operated by the SAO for and on behalf of NASA under contract NAS8-03060.

REFERENCES

Agius, N. K., Sansom, A. E., Popescu, C. C., et al. 2013, MNRAS, 431, 1929
Alatalo, K., Davis, T. A., Bureau, M., et al. 2013, MNRAS, 432, 1796
Amblard, A., Riguccini, L., Temi, P., et al. 2014, ApJ, 783, 135
Annibali, F., Bressan, A., Rampazzo, R., Zeilinger, W. W., & Danese, L. 2007, A&A, 463, 455
Auger, M. W., Treu, T., Gavazzi, R., et al. 2010, ApJL, 721, L163
Boroson, B., Kim, D.-W., & Fabbiano, G. 2011, ApJ, 729, 12
Bruzual, G., & Charlot, S. 2003, MNRAS, 344, 1000
Calzetti, D. 1997, in AIP Conf. Ser. 408, ed. W. H. Waller (Melville, NY: AIP), 403
Calzetti, D., Kinney, A. L., & Storchi-Bergmann, T. 1994, ApJ, 429, 582
Caon, N., Macchetto, D., & Pastoriza, M. 2000, ApJS, 127, 39
Cappellari, M., Verolme, E. K., van der Marel, R. P., et al. 2002, ApJ, 578, 787
Cardelli, J. A., Clayton, G. C., & Mathis, J. S. 1989, ApJ, 345, 245
Carlberg, R. G. 1984, ApJ, 286, 403
Crocker, A. F., Bureau, M., Young, L. M., & Combes, F. 2008, MNRAS, 386, 1811
Dale, D. A., & Helou, G. 2002, ApJ, 576, 159
David, L. P., Lim, J., Forman, W., et al. 2014, ApJ, 792, 94
Davis, T. A., Alatalo, K., Sarzi, M., et al. 2011, MNRAS, 417, 882
Denicoló, G., Terlevich, R., Terlevich, E., Forbes, D. A., & Terlevich, A. 2005, MNRAS, 358, 813
Desert, F.-X., Boulanger, F., & Puget, J. L. 1990, A&A, 237, 215
de Vaucouleurs, G., de Vaucouleurs, A., Corwin, H. G., Jr., et al. 1991, Third Reference Catalogue of Bright Galaxies, Vol. I, II, III (New York: Springer)
Di Matteo, P., Bournaud, F., Martig, M., et al. 2008, A&A, 492, 31
Di Matteo, P., Combes, F., Melchior, A.-L., & Semelin, B. 2007, A&A, 468, 61
Di Matteo, T., Springel, V., & Hernquist, L. 2005, Natur, 433, 604
Ekers, R. D., Wall, J. V., Shaver, P. A., et al. 1989, MNRAS, 236, 737
Ellis, S. C., & O'Sullivan, E. 2006, MNRAS, 367, 627
Emsellem, E., Cappellari, M., Krajnović, D., et al. 2007, MNRAS, 379, 401
Emsellem, E., Cappellari, M., Krajnović, D., et al. 2011, MNRAS, 414, 888
Fabbiano, G., Elvis, M., Markoff, S., et al. 2003, ApJ, 588, 175
Ferreras, I., & Silk, J. 2000, ApJ, 532, 193
Forbes, D. A. 1991, MNRAS, 249, 779
Forbes, D. A., Reitzel, D. B., & Williger, G. M. 1995, AJ, 109, 1576
Foster, C., Proctor, R. N., Forbes, D. A., et al. 2009, MNRAS, 400, 2135
Franx, M., & Illingworth, G. D. 1988, ApJL, 327, L55
Garcia, A. M. 1993, yCat, 410, 47
Gaspari, M., Brighenti, F., & Temi, P. 2012, MNRAS, 424, 190
Gaspari, M., Brighenti, F., & Temi, P. 2015, A&A, 579, A62
Giovannoli, E., Buat, V., Noll, S., Burgarella, D., & Magnelli, B. 2011, A&A, 525, A150
Goudfrooij, P., de Jong, T., Norgaard-Nielsen, H. U., Hansen, L., & Jorgensen, H. E. 1990, A&A, 228, L9
Grillo, C., Gobat, R., Lombardi, M., & Rosati, P. 2009, A&A, 501, 461
Heckman, T. M. 1980, A&A, 87, 152
Hopkins, P. F., Cox, T. J., Dutta, S. N., et al. 2009, ApJS, 181, 135
Howell, J. H. 2005, AJ, 130, 2065
Huchra, J. P., & Geller, M. J. 1982, ApJ, 257, 423
Ilbert, O., Salvato, M., Le Floc'h, E., et al. 2010, ApJ, 709, 644
Kaviraj, S., Schawinski, K., Devriendt, J. E. G., et al. 2007, ApJS, 173, 619
Kawata, D. 2001, ApJ, 558, 598
Kim, D.-W. 1989, ApJ, 346, 653
Kobayashi, C. 2004, MNRAS, 347, 740
Koleva, M., Prugniel, P., de Rijcke, S., & Zeilinger, W. W. 2011, MNRAS, 417, 1643
Komossa, S., Böhringer, H., & Huchra, J. P. 1999, A&A, 349, 88
Kuntschner, H., Emsellem, E., Bacon, R., et al. 2010, MNRAS, 408, 97
La Barbera, F., Ferreras, I., de Carvalho, R. R., et al. 2011, ApJL, 740, L41
Larson, R. B. 1976, MNRAS, 176, 31
Le Borgne, D., Rocca-Volmerange, B., Prugniel, P., et al. 2004, A&A, 425, 881
Lees, J. F., Knapp, G. R., Rupen, M. P., & Phillips, T. G. 1991, ApJ, 379, 177
Li, Z., Han, Z., & Zhang, F. 2007, A&A, 464, 853
Malin, D. F. 1985, in New Aspects of Galaxy Photometry, Vol. 232, ed. J.-L. Nieto (Berlin: Springer) doi:10.1007/bfb0030913
Maraston, C. 2005, MNRAS, 362, 799
Maraston, C., Daddi, E., Renzini, A., et al. 2006, ApJ, 652, 85
Marino, A., Rampazzo, R., Bianchi, L., et al. 2011, MNRAS, 411, 311
Mathews, W. G., & Brighenti, F. 2003, ARA&A, 41, 191
Mathews, W. G., Temi, P., Brighenti, F., & Amblard, A. 2013, ApJ, 768, 28
Morganti, R., de Zeeuw, P. T., Oosterloo, T. A., et al. 2006, MNRAS, 371, 157
Morrissey, P., Conrow, T., Barlow, T. A., et al. 2007, ApJS, 173, 682
Mulchaey, J. S., & Jeltema, T. E. 2010, ApJL, 715, L1
Nagar, N. M., Falcke, H., & Wilson, A. S. 2005, A&A, 435, 521
Noll, S., Burgarella, D., Giovannoli, E., et al. 2009, A&A, 507, 1793
O'Sullivan, E., Combes, F., Hamer, S., et al. 2015, A&A, 573, A111
Phillips, M. M., Jenkins, C. R., Dopita, M. A., Sadler, E. M., & Binette, L. 1986, AJ, 91, 1062
Pilbratt, G. L., Riedinger, J. R., Passvogel, T., et al. 2010, A&A, 518, L1
Pipino, A., D'Ercole, A., Chiappini, C., & Matteucci, F. 2010, MNRAS, 407, 1347
Pipino, A., D'Ercole, A., & Matteucci, F. 2008, A&A, 484, 679
Poglitsch, A., Waelkens, C., Geis, N., et al. 2010, A&A, 518, L2
Prandoni, I., Laing, R. A., de Ruiter, H. R., & Parma, P. 2012, JPhCS, 372, 012067
Raimann, D., Storchi-Bergmann, T., Bica, E., & Alloin, D. 2001, MNRAS, 324, 1087
Rawle, T. D., Smith, R. J., & Lucey, J. R. 2010, MNRAS, 401, 852
Rieke, G. H., Young, E. T., Engelbracht, C. W., et al. 2004, ApJS, 154, 25
Salpeter, E. E. 1955, ApJ, 121, 161
Sánchez-Blázquez, P., Forbes, D. A., Strader, J., Brodie, J., & Proctor, R. 2007, MNRAS, 377, 759
Sandage, A., & Bedke, J. 1994, The Carnegie Atlas of Galaxies, Vol. I, II (Washington, DC: Carnegie Institution of Washington Publication)
Sarzi, M., Alatalo, K., Blitz, L., et al. 2013, MNRAS, 432, 1845
Sarzi, M., Falcón-Barroso, J., Davies, R. L., et al. 2006, MNRAS, 366, 1151
Serra, P., Amblard, A., Temi, P., et al. 2011, ApJ, 740, 22
Serra, P., Oosterloo, T., Morganti, R., et al. 2012, MNRAS, 422, 1835
Serra, P., & Oosterloo, T. A. 2010, MNRAS, 401, L29
Serra, P., & Trager, S. C. 2007, MNRAS, 374, 769
Serra, P., Trager, S. C., Oosterloo, T. A., & Morganti, R. 2008, A&A, 483, 57
Shanks, T., Metcalfe, N., Chehade, B., et al. 2015, MNRAS, 451, 4238
Siebenmorgen, R., Freudling, W., Krügel, E., & Haas, M. 2004a, A&A, 421, 129
Siebenmorgen, R., Krügel, E., & Spoon, H. W. W. 2004b, A&A, 414, 123
Sil'chenko, O. K. 2006, ApJ, 641, 229
Slee, O. B., Sadler, E. M., Reynolds, J. E., & Ekers, R. D. 1994, MNRAS, 269, 928
Smith, D. J. B., & Hayward, C. C. 2015, MNRAS, 453, 1597
Smith, M. W. L., Gomez, H. L., Eales, S. A., et al. 2012, ApJ, 748, 123
Spiniello, C., Koopmans, L. V. E., Trager, S. C., Czoske, O., & Treu, T. 2011, MNRAS, 417, 3000
Spolaor, M., Kobayashi, C., Forbes, D. A., Couch, W. J., & Hau, G. K. T. 2010, MNRAS, 408, 272
Spolaor, M., Proctor, R. N., Forbes, D. A., & Couch, W. J. 2009, ApJL, 691, L138
Springel, V., Di Matteo, T., & Hernquist, L. 2005a, ApJL, 620, L79
Springel, V., Di Matteo, T., & Hernquist, L. 2005b, MNRAS, 361, 776
Tal, T., van Dokkum, P. G., Nelan, J., & Bezanson, R. 2009, AJ, 138, 1417
Temi, P., Brighenti, F., & Mathews, W. G. 2007a, ApJ, 660, 1215
Temi, P., Brighenti, F., & Mathews, W. G. 2007b, ApJ, 666, 222
Temi, P., Brighenti, F., & Mathews, W. G. 2009, ApJ, 695, 1
Temi, P., Mathews, W. G., & Brighenti, F. 2005, ApJ, 622, 235
Thomas, D., Maraston, C., & Bender, R. 2003, MNRAS, 339, 897
Tingay, S. J., & Edwards, P. G. 2015, MNRAS, 448, 252
Tingay, S. J., Edwards, P. G., & Tzioumis, A. K. 2003, MNRAS, 346, 327
Tonry, J. L., Dressler, A., Blakeslee, J. P., et al. 2001, ApJ, 546, 681
Tortora, C., Napolitano, N. R., Cardone, V. F., et al. 2010, MNRAS, 407, 144
Tortora, C., Pipino, A., D'Ercole, A., Napolitano, N. R., & Matteucci, F. 2013, MNRAS, 435, 786
Trager, S. C., Faber, S. M., Worthey, G., & González, J. J. 2000, AJ, 120, 165
Treu, T., Auger, M. W., Koopmans, L. V. E., et al. 2010, ApJ, 709, 1195

Vazdekis, A., Cenarro, A. J., Gorgas, J., Cardiel, N., & Peletier, R. F. 2003, MNRAS, 340, 1317
Wang, Z., Kenney, J. D. P., & Ishizuki, S. 1992, AJ, 104, 2097
Werner, N., Oonk, J. B. R., Sun, M., et al. 2014, MNRAS, 439, 2291
White, S. D. M. 1980, MNRAS, 191, 1
Wiklind, T., Combes, F., & Henkel, C. 1995, A&A, 297, 643
Wiklind, T., & Henkel, C. 1989, A&A, 225, 1
Williams, T. B., & Schwarzschild, M. 1979, ApJS, 41, 209
Young, L. M., Bureau, M., Davis, T. A., et al. 2011, MNRAS, 414, 940
Zhang, Y., Gu, Q.-S., & Ho, L. C. 2008, A&A, 487, 177